Article:
Tian, Y., Yang, X., Ma, L. orcid.org/0000-0002-3731-8464 et al. (2 more authors) (2024) Understanding the effects of mesh smoothing methods in the CFD modelling of Zhundong lignite ash deposition. Fuel, 364. 131077. ISSN: 0016-2361

https://doi.org/10.1016/j.fuel.2024.131077

Fuel 364 (2024) 131077

Contents lists available at ScienceDirect

Fuel

journal homepage: www.elsevier.com/locate/fuel

Full length article

Understanding the effects of mesh smoothing methods in the CFD modelling of Zhundong lignite ash deposition

Yufei Tian [a], Xin Yang [b,c], Lin Ma [a,*], Derek Ingham [a], Mohamed Pourkashanian [a]

[a] Energy 2050, Department of Mechanical Engineering, University of Sheffield, Sheffield, S10 2TN, UK
[b] School of Mechatronical Engineering, Beijing Institute of Technology, Beijing, 100811, China
[c] Yangtze Delta Region Academy, Beijing Institute of Technology, Jiaxing, 314000, China

ARTICLE INFO

Keywords:
CFD
Ash deposition
Dynamic mesh
Mesh smoothing

ABSTRACT

Slagging and fouling are the most typical causes of unscheduled solid fuel boiler shutdowns. The CFD-based prediction of the deposit growth and rates, which combine the basic mechanisms of ash particle transport, impaction, sticking, as well as the complex aerodynamics of a boiler, is helpful to optimize the design and operation of boilers. In this study, a dynamic CFD model, which contains the molten fraction based sticking model and dynamic mesh model, is developed and validated in Zhundong lignite combustion in a pilot-scale furnace. With the employment of this model, a smooth growth of deposition and an accurate simulation can be achieved without applying the mesh smoothing strategy. Further, the predicted results are in good agreement with the experimental data. The effects of two mesh smoothing methods, which are the mass spreading algorithm and the group-averaged redistribution method, have been investigated under different furnace operation conditions. Compared to the simulations without the smoothing methods, a smaller particle count is required during the simulation to obtain the accurate, efficient and stable predicted results. The smoothing methods make a small difference (within 3.0%) on the predicted heat flux and deposition rate. In contrast, the deposition thickness at the tube position $\alpha = 180°$ after two deposition hours would be within 16.8% smaller compared to the predicted results without the smoothing methods.

1. Introduction

In the near future, it is anticipated that the use of pulverized solid fuel will continue to grow. Technologies that utilized pulverized solid fuel as a co-firing fuel will prove indispensable to meet the electricity demands as well as to combat the ever-increasing threat of global warming, especially in countries where fossil fuels remain the major of energy source [1]. However, changing the fuel mixture to be used in the existing boiler can result in a radically different ash deposition behaviour. Ash deposition is a major concern in the daily operation of boilers [2,3]. If the deposition layer is allowed to grow to a sufficient degree, it would impede the effective heat transfer of the combustion system [2,4]. In addition, the continuous ash deposition in the boilers would not only restrict the flow of the flue gases but also corrode the furnace and the tubes [5–8]. Furthermore, ash deposit removal is essential to ensure the maximum boiler heat transfer efficiency. Typically, the soot blowing is periodically used to remove most of the deposition [6]. If the deposition has not been completely removed, it could continue to grow. When the deposit has grown to a sufficient size, manual cleaning is needed, which, obviously, would require boiler to be shutdown. This, of course, would increase the boiler operational costs [6,8]. For these reasons, it is necessary to develop numerical models to simulate the ash deposition characteristics, which in turn will guide the choice on the design parameters to minimize the risk of the unstable operation of the boilers.

The formation of ash deposit results from several key physical processes that account for ash generation, transport and deposition. The role of the transport and deposition phase can be predicted by examining the time history of the ash particles, which further involves mechanisms that allow the ash to deposit on solid walls (e.g. particle transport, particle impaction and sticking, deposit growth and etc.) [9,10]. In the later stage of the ash deposit formation, the shedding of the ash deposit, which could be caused by erosion, gravitational force, thermal stresses, soot blowing, etc., is another significant phenomenon [3,6]. In the CFD methods, a global computational domain is constructed and is used to capture the deposition process at the macroscopic level to account for both the steady and dynamic phenomena. Several sub models are also developed and employed while modelling the processes of the ash deposition growth during the solid fuel combustion in the

* Corresponding author.
E-mail address: lin.ma@sheffield.ac.uk (L. Ma).

https://doi.org/10.1016/j.fuel.2024.131077
Received 13 December 2023; Received in revised form 18 January 2024; Accepted 24 January 2024
Available online 1 February 2024

boiler. For instance, the flue gas flow in the boiler is modelled by the RANS approach, while the ash particle trajectories are modelled by the DPM module through the Lagrangian approach [3,11–13]. Ash particle sticking models need to take the viscosity of the ash particles, the kinetic energy of the impacting particles and the molten degree of the ash particles into consideration [14]. Some common sticking models are the viscosity-based sticking model [14–21], kinetic energy sticking model [2,3,22,23] and molten fraction sticking model [12,24–26]. Additionally, the dynamic mesh model can also be employed to predict the growth of the ash deposition [27–31].

In this field of research concerning the ash deposition prediction, two broad approaches can be identified, which can be coined as steady and dynamic [3]. Steady simulations refer to the rate of the deposit accumulation and the deposition behaviours are assumed constant throughout the growth period; this is in contrast with the dynamic simulations in which the rate and the behaviours are dynamically computed and updated at each time step. The steady simulations provide a good approximation to problems where the temperature on the deposition site is close to the furnace temperature [4,14,17,32,33]. A dynamic approach is generally used, however, when there is an appreciable temperature gradient present at the deposition site which can greatly influence the local deposition behaviour. Under such a case, the model variables need to be constantly updated depending on the growth stage of the deposit [26,27,29,30,34,35].

To predict the ash deposition more accurately, the deposit growth could be directly implemented into the CFD modelling, which means that the deposit will grow according to the accumulated mass of the particles that has been collected on the deposit surfaces. Simulating such an effect can be divided into two steps. The first step is to calculate the accumulated mass on each of the mesh faces, which can be determined by the ash particles' physical properties, their trajectories and particles impaction and sticking efficiency. The second step is then to mimic the deposition growth by morphing the interface geometry so as to simulate the effect of the mass deposit in a continuous manner. To achieve this, one can employ a mesh motion procedure on the deposition surface based on the collected mass on each of the mesh faces. In ANSYS FLUENT, the outward growth of the deposit is performed by translating the interface nodes in the normal direction of the initial geometry. The amount of displacement produced by the translation is a function of the local mass flux. This can be controlled by a dynamic mesh panel and UDFs. The effect of turbulence is to introduce a stochastic process that mimics the inherent random nature of the fluid flow. One consequence of turbulence is the uneven distribution of the number of impacting particles despite the symmetry of the initial configuration. Consequently, a given face may not have collected any ash particles whereas its neighbouring face may have collected several. The naive implementation of the node update procedure based on this observation would lead to a highly discontinuous mass distribution, which could deteriorate the quality of the interface mesh cells to a point where negative volume cells might appear, which can lead to other numerical problems such as stability and convergence in the solution procedure [27]. One way to resolve those issues is to use a finer mesh and to increase the number of tracked particles. However, this may lead to a massive increase in the computational costs. To overcome this problem, García Pérez et al. [27] developed a mass spreading algorithm, which regulates how the mass is redistributed around the adjacent surface. Yang et al. [29] also used the similar multiple-point weighted moving average algorithm when dynamically modelling the biomass ash deposition. In addition, Zhou et al. [30] investigated the growth of the ash deposition on a temperature-controlled probe in a pilot-scale furnace with CFD modelling. Another smoothing method was developed in the Ref. [30], in which the grid faces of the deposition surface were divided into sub-groups with the averaged growth rate in each group and then redistributed the growth of each face group by the weighed mean method. A similar smoothing strategy was used by Zheng et al. [31,36] in the dynamic ash deposition model.

Table 1
Fuel properties of the Zhundong lignite [37].

Ash composition (wt.%)		Proximate analysis (wt.%) (db)	
SiO_2	35.08	Volatiles	32.79
Al_2O_3	14.04	Fixed carbon	52.91
Fe_2O_3	6.07	Ash	12.3
CaO	27.78	HHV (MJ/kg) (db)	54.01
MgO	4.73	Ultimate analysis (wt.%)	
K_2O	0.48	C	64.07
Na_2O	8.31	H	3.58
TiO_2	0.71	O	19.22
SO_3	2.80	N	0.65

Although the mesh smoothing algorithm is reasonably accurate and can avoid creating negative cells during the node update, it is, however, quite difficult to implement in a parallelized machine. Since the redistribution requires access to neighbouring surfaces, a UDF macro needs to be hard-coded into the simulation, which causes extra work for the multiple processors to synchronize [28]. This may increase the difficulty for a complete simulation case, as well as affecting the accuracy of the deposition profiles due to the smoothing process. It is noted that Yang et al. [29] has successfully employed the mesh smoothing method in a parallel CFD solver by generating an order list to obtain the index list of the looping face connectivity and physical face connectivity of the grid faces at the interface based on the face-looping macro. Currently, the mesh smoothing methods are often used in modelling the growth of ash deposition to avoid the mesh instabilities and model crashes. But the exact effects of the smoothing strategy to the deposition rate, deposition thickness and heat flux through the deposit surface during the ash deposition simulation are still not clear.

Therefore, this study aims to firstly develop a novel dynamic CFD model to predict the ash deposition formation without using the smoothing methods, and secondly investigate the effects of the existing mesh smoothing strategies during the simulation of the ash deposition processes. In particular, we focus on the effects of the various smoothing methods on the deposition rate, thickness, and heat flux across the surface. It is worth pointing out that although the deposition process in the boilers is a 3D phenomenon, a 2D model is employed in this paper to reduce the computational cost. This is justified since several studies have found that 2D models have managed to produce reasonable numerical results that match with the experimental data [2,13,27]. The experimental data of ash deposition in Zhundong lignite combustion from the pilot-scale furnace located in the Zhejiang University [37] has been used to develop and test the model.

2. Source of experimental data

To validate and develop the models, the 300 kW pulverized fuel combustion furnace located at Zhejiang University has been utilized to provide experimental data. The pilot-scale furnace is a down-fired furnace of a cylindrical shape with a length of 3950 mm and an inner diameter of 350 mm. The furnace is fitted with a swirl burner, which consists of a primary and secondary register. Pulverized fuels and primary oxidizer stream are delivered via the primary register while the rest of the preheated oxidizer are fed through the secondary register. Additionally, there are three cooled ash deposition probes inserted into the furnace centre, which have furnace temperatures of approximately from 1373 K to 1593 K. The probes are made of stainless steel and cooled by the cooling oil with the temperature controlled at 503 K, which is assumed as the inner temperature of the probe during the simulation. Meanwhile, the deposit growth is online monitored by the image sampling system. Readers are referred to the work of Zhou et al. [37] for more information on the whole experimental set-up.

Table 1 shows the fuel properties of the Zhundong lignite that was used in the experiments. The ash composition is identified to compose mostly of SiO_2, CaO, Al_2O_3 and Na_2O, and these main compositions

are regarded as playing a crucial role in the deposit formation process [12,37]. In this study, a typical deposition time of the first two hours is used to ensure that the deposits have sufficient mass to allow a distinct shape to be distinguished before excessive mass is shed, as the obvious shedding appears after approximately two hours of deposition time. Currently, the developed model ignores shedding. Therefore, a reasonable improvement to the prediction model is to incorporate a shedding model, which should be capable of predicting the shedding rate and the resulting geometry of the deposit. However, this may be considered in a future work.

3. Mathematical models and simulation methods

3.1. Discrete phase model

The essential ingredient in modelling the formation of ash deposit is to understand how the ash particles are transported to the deposit sites. The arrival rate of the particles on the deposit site depends on the ash particle trajectories. For modelling purposes, the ash particles can be treated as Lagrangian particles, which means the ash particles are treated as point masses and whose equations of motion are prescribed in the Lagrangian frame. FLUENT models these particles via the Discrete Phase Model (DPM) module in which the trajectories are determined by the momentum conservation principle. The kinematic equations satisfied by a Lagrangian particle are obtained via the momentum balance in each component. Let $\vec{v}_p$ denote the velocity vector of a Lagrangian particle and $\vec{v}_g$ be the background gas flow velocity, then the rate of change of $\vec{v}_p$ is given by [12]:

$$\frac{d\vec{v}_p}{dt} = \frac{18\mu_g}{\rho_p d_p^2}\frac{C_D Re_p}{24}\left(\vec{v}_g - \vec{v}_p\right) + \vec{g}\frac{\left(\rho_p - \rho_g\right)}{\rho_p} + \vec{F} \tag{1}$$

Here, ρ_p and ρ_g denote the density of the particle and gas, respectively. μ_g is the dynamic viscosity, d_p is the characteristic diameter of the particles, C_D is the drag coefficient, Re_p is the particle's Reynolds number and $\vec{g}$ is the acceleration due to gravity. Moreover, other additional forces, such as thermophoresis force and Brownian force, can be modelled by including a source term, i.e. $\vec{F}$, to the equations. In this study, the thermophoretic force, which is caused by the temperature gradient in the gas that is close to the solid deposition surface, is considered since the ash deposition on a cooled surface is modelled. However, the direct condensation of the alkali vapour released from the Zhundong lignite is not considered. This is because its contribution of the deposition only accounts for around 2% in the initial stage and that reduces to 0.1% in the final stage [12]. In addition, the effect of turbulent diffusion is considered by the Discrete Random Walk (DRW) model, which integrates the particle motion equation of a large number of particles using the instantaneous fluid velocity. Preliminary studies have revealed that the DRW allows the impacting particles to expand on the two sides of the cylindrical probe to a significant degree and causes the particles to impact on the furnace wall [3]. Further, the effects of particle–particle interaction are ignored as well as the influence on the turbulence diffusion due to the particles' presence. This is an acceptable compromise provided that the volume fraction of the fly ash particles in the flue gas is relatively low [38].

3.1.1. Sticking model

Sticking may occur when an ash particle arrives at the impaction surface. However, not all impacting particles will adhere to the surface — only a fraction of the particles will do so. The sticking efficiency, defined as the ratio between the number of sticking particles and the total number of impacting particles, depends on several factors, such as the physical and kinematic properties of the impacting particles as well as the properties of the deposition surfaces. Wieland et al. [14] identified the key variables that relate to the sticking process of the ash particles. These are the viscosity of the ash particles, the kinetic energy of the impacting particles and the molten degree of the ash particles. The viscosity-based model requires the specification of the reference viscosity. Depending on the furnaces being used, the same fuel (e.g. Bituminous US coal) can result in a vastly different reference value [14–16,21]. When using the kinetic energy threshold sticking model, some important parameters require careful tuning between the experimental data and the simulation result in order to produce an acceptable accuracy [3]. In this study, the molten fraction based sticking model is employed to estimate the sticking efficiency of the ash particles. In this method, the melt fractions of both the particles and the deposit on the deposition site are computed based on the thermodynamic equilibrium state, which is determined by a minimization process applied to the Gibbs energy in the system with mass balance constraints [12,25]. Denote $\eta_p\left(T_p\right)$ and $\eta_s\left(T_s\right)$ be the melt fractions of the ash particles and the deposit on the deposition surface at the particle temperature T_p and surface temperature T_s, respectively, then the sticking efficiency, η_{stick}, may be computed as follows:

$$\eta_{\mathrm{stick}} = \eta_p(T) + \left(1 - \eta_p(T)\right)\eta_s\left(T_s\right) \tag{2}$$

The thermodynamic equilibrium is calculated by the thermodynamic software package FactSage 7.0, and the predicted results of melt fraction for the original coal ash can be found in Ref. [3].

3.1.2. Ash deposition growth model and deposition properties

The deposit growth is simulated by means of a node translation on the deposit-flow interface according to the mass that has been collected on each of the faces over an accretion period. ANSYS FLUENT offers the dynamic mesh model to simulate the growth of the ash deposition on the deposit surface. The motion of these nodes is implemented by employing an in-house developed UDF. The increased thickness of the ash deposition $\Delta\delta_i$ on face i of the interface can be calculated over a time interval Δt as follows:

$$\Delta\delta_i = \frac{\Delta m_i}{\rho_p\left(1 - \varepsilon_{\mathrm{deposit}}\right)S} \tag{3}$$

where Δm_i is the accumulated deposition mass on the i-th surface segment over the interval, S is the surface area of this segment and ρ_p is the density of the ash particles. The variable $\varepsilon_{\mathrm{deposit}}$ is the porosity of the ash deposition.

The average value of the thickness of the ash deposition on the two adjacent faces is used to determine the new coordinates of the nodes. This means that the motion of each node of the interface between the flue gas and the deposit face is calculated from the average collected mass from its two adjacent faces. Shown in the Eq. (4), $\Delta\bar{\delta}_i$ represents the average value of the thickness of the ash deposition on the two neighbouring faces; $\Delta\delta_i$ and $\Delta\delta_{i-1}$ are the increased thickness of these two adjacent faces:

$$\Delta\bar{\delta}_i = \frac{\Delta\delta_i + \Delta\delta_{i-1}}{2} \tag{4}$$

A fixed direction, normal to the initial flow-deposit interface, is constrained on the growth direction of the nodes. At the end of the accretion period, the nodes are relocated along the normal of the cylindrical tube. Let $\left(x_i^t, y_i^t\right)$ denote the position vector of the i-th node on the interface boundary at the time t, then the new position after the node update, namely $\left(x_i^{t+\Delta t}, y_i^{t+\Delta t}\right)$, may be computed by:

$$x_i^{t+\Delta t} = x_i^t + \Delta\bar{\delta}_i\cos\theta_i \tag{5}$$

$$y_i^{t+\Delta t} = y_i^t + \Delta\bar{\delta}_i\sin\theta_i \tag{6}$$

where $\Delta\bar{\delta}_i$ is calculated from Eq. (4) and θ_i is the azimuthal angle of the i-th node.

With the deposit growth, the deposition properties, such as porosity, thermal conductivity, deposition surface temperature etc, would change [12]. In principle, however, the deposit porosity can vary depending on the deposit temperature and its chemical composition. Zheng et al. [31,36] assumed that the porosity of the ash deposit is a linearly decreasing function of the thickness of the ash deposition. In

this paper, in order to account for the temperature variation on $\epsilon_{\text{deposit}}$, a simple correlation based on the ratio of the liquid to the solid volumes can be employed [26]. More specifically, let V_{liquid} and V_{solid} denote the volume of the liquid and solid phase, respectively, then the porosity is given as follows [12,18,33]:

$$\epsilon_{\text{deposit}} = 1 - \left[(1 - \epsilon_0) + \frac{V_{\text{liquid}}}{V_{\text{solid}}} (1 - \epsilon_0) \right] \tag{7}$$

where ϵ_0 is the initial deposit porosity. The effect of the deposition temperature is to alter the volume fraction of the liquid and solid phases. In addition, the heat conduction in the deposit layer is directly resolved by the CFD solver. One of the critical parameters, the thermal conductivity of the deposit layer, which is considered as a linear function of the thickness of ash deposit, can be determined by the experimental data [37].

3.2. Integration of the ash deposition model into the CFD framework

ANSYS FLUENT version 19.2 has been employed to predict the ash deposition formation of Zhundong lignite combustion. The software is combined with in-house developed UDFs. The realizable $k - \epsilon$ model is incorporated to simulate the effect of turbulence and the Discrete Ordinate model is used for the radiation heat transfer. Finally, the Discrete Phase Model (DPM) is used for the ash particle tracking. The DRW model is also applied to simulate the effect of turbulence on the ash particles. In addition, the particle sticking model and the ash deposition growth model are employed to predict the ash particle sticking behaviour and the ash deposition growth. A two-dimensional (2D) geometry with a tube of diameter 40 mm placed in the central region is considered as the computational domain, which is shown in Fig. 1. The length of this computational domain is 700 mm with a width of 350 mm [12]. The tube is surrounded initially with a deposit layer of 1 mm [30]. The unstructured mesh is used, and the computational domain consists of a solid zone and a fluid zone. The triangular grids are used in the computational domain to apply the dynamic mesh method, whereas the quadrilateral grids surround the both side of the deposit-flow interface to obtain the accurate resolving of the flow field of this deposition surface and the heat conduction in the solid zone. The size of the quad meshes around the interface at the fluid side is approximately 0.1 mm, which suggested by [13,39]. The ash particles are assumed to be uniformly distributed at the inlet and they are injected from a section of the inlet boundary spanning 60 mm about the line of symmetry. The reason to limit the injection length is to reduce the particle count since only particles that interact with the tube contribute to the deposit growth. The boundary conditions of the flue gas are determined from the combustion cases. The flow rate of 1.153 g/s was used for the ash particles and the flue gas is assumed to consist of N_2-0.758, CO_2-0.166, O_2-0.05 and H_2O-0.026 in mole fraction. The sizes of ash particles ranged between 1 μm and 60 μm with a mean diameter of 16 μm and a spread parameter of 0.7 based on the Rosin-Rammler distribution, which indirectly results from the original coal particle size distribution and the ash content [12,37]. Since the ash deposition rate is obtained through the above modelling, the deposition growth model can be applied to simulate the growth of the ash deposition on the deposit surface. The motion of the nodes in the fluid–solid interface (terms as the deposit surface) is modified by the dynamic mesh model in conjunction with the 'DEFINE_GRID_MOTION' UDF macro. It is noted that parameters in the dynamic mesh model have been carefully selected to minimize the instability. For example, in the spring-based smoothing method, the spring constant factor is set to 0.1, which is found to produce stable results [40]. As for the remeshing module, the minimum and maximum length scale are set to 0.00026 m and 0.0005 m for the deposit solid zone [40].

The flow chart of the simulation algorithm is shown in Fig. 2. A similar quasi-transient calculation concept has been used to integrate the deposition growth model with the CFD framework [3,26]. In each time step, the algorithm proceeds to compute the global gas flow properties, such as the flow velocity, temperature, wall heat flux, etc. Once the velocity fields are known, Lagrangian particles are released from the inlet and are subsequently tracked by computing their trajectories. The sticking procedure applies to a Lagrangian particle on the deposition surface, which determines a percentage of the mass of the particle that will stick to the surface. The collective mass on a deposition surface is then used to update the surface node dynamically and a global meshing is subsequently performed. In the next time step, the CFD calculations and mesh updating will continue on the updated mesh in the previous time step.

Due to the large number of cells in the computational domain, it has become a general requirement to utilize the parallelization capability of the modern computer to accelerate the solution procedure. Note, however, that the deposit-flow interface would be separated in different partitions and solved through different processes, when the default partition method Metis is applied in the parallel FLUENT. This may result in the erroneous mesh update if the dynamic mesh model was enabled in the simulation. Therefore, the built-in Polar R-Coordinate partition method is employed to ensure the deposit-flow interface (known as deposit surface) placed into the same partition. In doing so, the dynamic mesh could be deployed in the parallel FLUENT mode to properly modify the interface node whilst retaining the same performance acceleration.

In the simulation, both the accuracy and the efficiency are important factors to take into consideration. A numerical independence study is carried out for the baseline case on a clean tube to examine the effect of mesh resolution and tracked particle count to the accuracy of the numerical solution. Three different meshes are included in the study - a coarse mesh with 1.4×10^4 cells and 100 faces on the interface, a medium mesh with 5.5×10^4 cells and 200 faces, and a fine mesh with 25×10^4 cells and 400 faces. In addition, the tracked particle count N is estimated to be 8×10^4 for the medium mesh in this study, since there are 40 injection points applied in the particle injection location and a particle size interval of 100 and 20 tries are implemented in the DRW module of FLUENT. The deposition efficiency, DE_f, at the grid face, is considered as an important indicator of the severity of ash deposition. This is used to compare the results of the independence studies of the tracked particle count and mesh resolution, since the numerical solution is found to be most sensitive to these two critical values. The mean differences, E_r, between these test cases are measured by the mean relative difference of DE_f. Moreover, DE_f and E_r are defined as follows:

$$DE_f = \frac{A_{\text{deposit}}}{A_{\text{inlet}}} \tag{8}$$

$$E_r = \frac{\sum_{i=1}^{n} \left| DE_{f_i,X} - DE_{f_i,Y} \right|}{n DE_{f_{max},Y}} \tag{9}$$

where A_{deposit} is the mass flux of the deposition ash particles at the clean tube, and the A_{inlet} is the mass flux at the inlet; $DE_{f_i,X}$ is the deposition efficiency of the test cases whilst $DE_{f_i,Y}$ is the deposition efficiency of the finest setting case in the independency study. $DE_{f_{max},Y}$ represents the largest deposition efficiency of the finest setting case, respectively. Fig. 3(a) shows the deposition efficiency DE_f under three different meshes. It can be observed that the results from the medium meshes are close to that of the fine meshes. The mean difference (E_r) between these two cases is 0.60%. For this reason, the medium mesh is chosen for this study. Furthermore, the relative difference in the deposition efficiency DE_f for the four particle counts is shown in Fig. 3(b). When the tracked particle count is increased from $0.25N$ to $2N$, a smoother profile in the deposition efficiency is observed. Indeed, this trend is reflected by the mean difference E_r, which sees a reduction of 4.56% to 0.70% when the particle count is changed from $0.25N$ to N.

From the result of the independency study, the DE_f in the case with the particle count of $0.25N$ appears to be not smooth compared

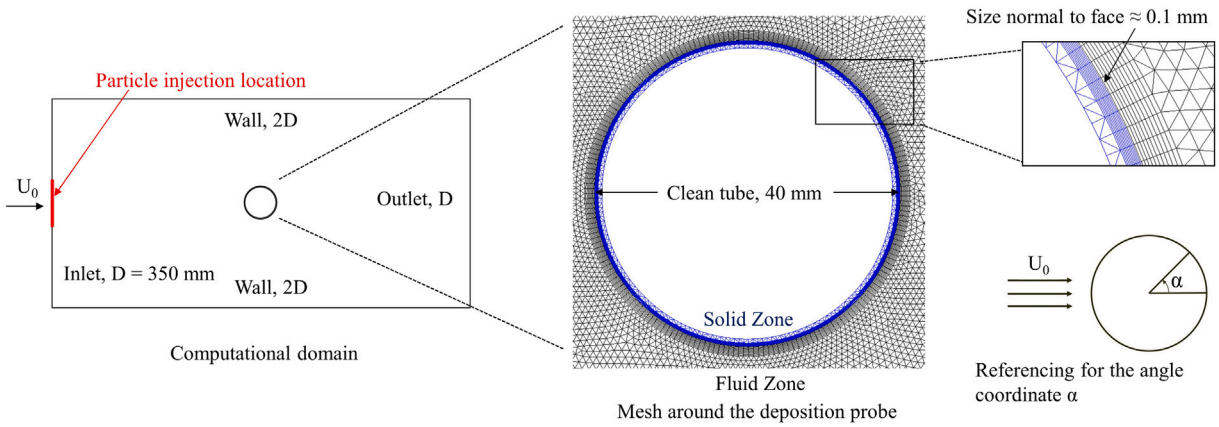

Fig. 1. Schematic diagram of the computational domain in Zhundong lignite combustion case.

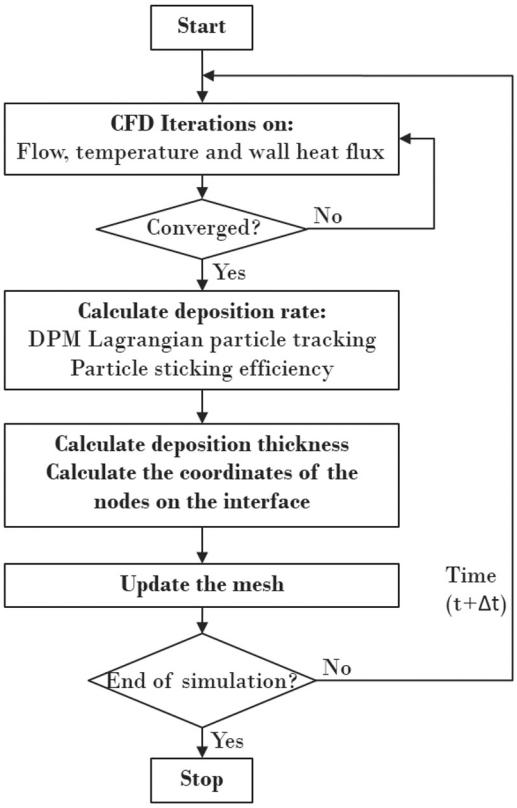

Fig. 2. The algorithm of the ash deposition growth model integration in the CFD framework.

to the cases with larger particle count. It appears that beyond a certain mesh resolution, saw-tooth instability could propagate throughout the simulation, which may pose a risk for the appearance of negative cell volumes during the mesh update. The appearance of the instability may be attributed to the non-smooth mass flux on the deposit surface, which is determined from the discrete phase. One way to resolve this issue is to employ the mass re-distribution approach, in which the mass of the impacting particle is re-distributed over a section of the interface surface. Another way is to increase the particle count to reduce the difference of the mass flux on the adjacent deposit faces. As for the mesh smoothing methods, there are two different smoothing algorithms chosen in this study. The smoothing method 1 is the mass spreading algorithm used by García Pérez et al. [27], and the smoothing method 2 is the group-averaged redistribution method used by Zhou et al. [30]. The details of these two smoothing methods are shown in Appendix A. In order to investigate the effects of the mesh smoothing method (also called the mass re-distribution strategy), multiple furnace operation conditions will be tested at various furnace temperatures ranging from 1373 K to 1593 K, the flue gas velocity ranging from 2.8 m/s to 15 m/s, and the mean particle sizes in the Rosim-Rammler distribution range from 5 μm to 25 μm. In each furnace operation condition, three different particle counts ($N, 0.5N$ and $0.25N$) will be considered during the simulation with two different mesh smoothing methods and without the smoothing method. That results in the total number of $9 \times 7 = 63$ CFD cases that would be investigated. More details of the simulated cases can be found in Appendix B.

4. Results and discussions

4.1. Validation

4.1.1. The baseline cases ($T_{gas} = T_{par} = 1543$ K, $V_{gas} = 2.8$ m/s, $d_{mean} = 16$ μm)

Fig. 4 shows the temperature contour of the solid zone for the deposition time of 0, 60 and 120 min. It can be seen that the deposition mainly occurs at the windward section of the tube and the largest thickness of the deposition is at the tube position of $\alpha = 180°$. The temperature of the deposit surface increases when the deposition grows. It can be seen that temperature at the outer deposit surface has nearly reached the flue gas temperature after 2 h. Fig. 5 shows the deposition thickness changed as a function of the deposition time and both the predicted results and the experimental data are included. It is noted that the deposition thickness is the values at the tube position $\alpha = 180°$. Generally, it can be observed that the predicted deposition thickness changes as a linear function of the deposition time. The deposition thickness is slightly over-predicted compared to the experimental results. When the deposition time is 2 h, the difference between the predicted deposition thickness and the experimental data is approximately 10.8%.

4.1.2. Heat transfer properties under different furnace temperature

The furnace temperature, which can affect not only the ash particle temperature but also the thermal boundary near the deposition surface, play an important role in the deposition formation. Fig. 6 shows the comparison of the heat flux between the predicted results and the experimental data under three different furnace temperatures as a function of the deposition time. Again, the representative heat flux value is taken at the upstream stagnation point of the tube. Generally, it can be observed that the predicted results are in reasonable agreements with the experimental data for the three cases. The similar variance trend is showed in these three curves, in which the heat flux decreases rapidly in the first 30 min and then slowly decreases in the later stage. This

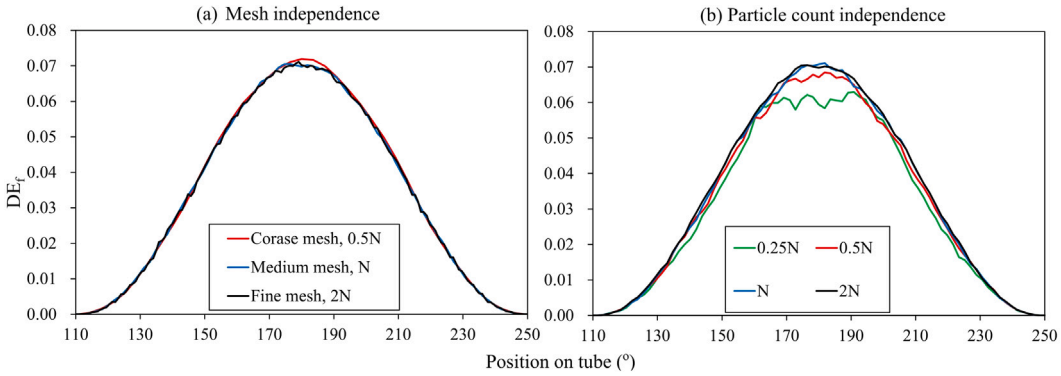

Fig. 3. Independence study of the baseline case: (a) Mesh independence; (b) Particle count independence.

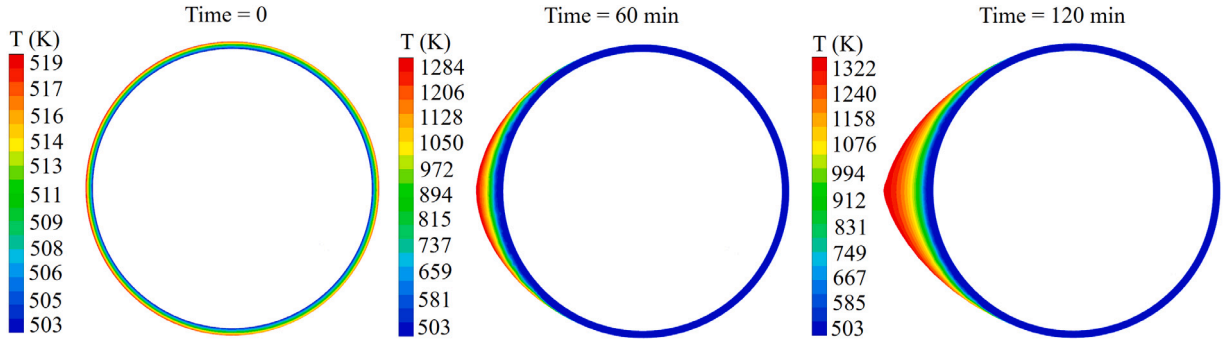

Fig. 4. Temperature contour of the solid zone (deposition and steel tube) for deposition time of 0, 60 and 120 min.

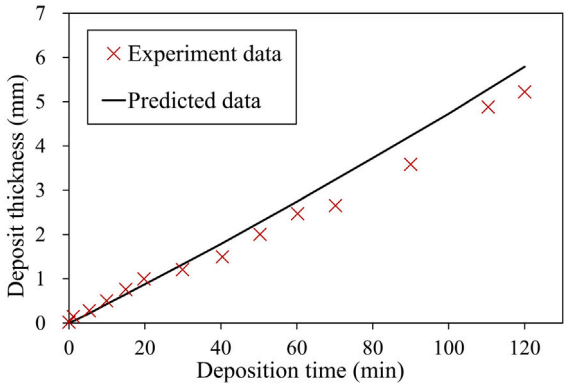

Fig. 5. Comparison of the deposition thickness between the predicted results and the experimental data as a function of the deposition time.

is mainly because the thermal conductivity of the deposit is relatively low in the initial stage compared to the steel tube. When the deposition time reaches two hours, the differences between the predicted heat flux and the experimental data under these three different furnace temperatures are both less than 15.2%. Moreover, the predictions also show that a higher heat flux is generally expected at higher furnace temperature. Based on the results in the validation part, an accurate and stable simulation can be obtained without the employment of the mesh smoothing methods.

4.2. Effects of mesh smoothing methods during different furnace operational conditions

The effects of the smoothing strategies to the deposition rate, deposition thickness and heat flux through the deposit surface during the ash deposition simulation are discussed in this section. Two different mesh smoothing strategies, which are the mass spreading algorithm [27] and the group-averaged redistribution method [30], are applied during the simulations.[1] Both the furnace temperatures, the flue gas velocities and the ash particle sizes are the important factors in the processes of the ash deposition formation. Hence, multiple furnace operation conditions will be tested to investigate the effects of the mesh smoothing methods.

Fig. 7 shows the predicted deposition thickness with different mesh smoothing methods under different furnace operational conditions. The similar variance trends, in which the deposition thickness would linearly increase as a function of time, can be observed in both Fig. 7(a)–(i). It can be observed that the predicted results with the smoothing methods are always smaller than the results without smoothing, while the results with the smoothing method 2 are even smaller. It is mainly

[1] Note: The results used to discuss the effects of mesh smoothing methods are obtained from the case with particle count of $0.5N$ when the smoothing methods are employed in the simulation. More details can be found in Appendix C.

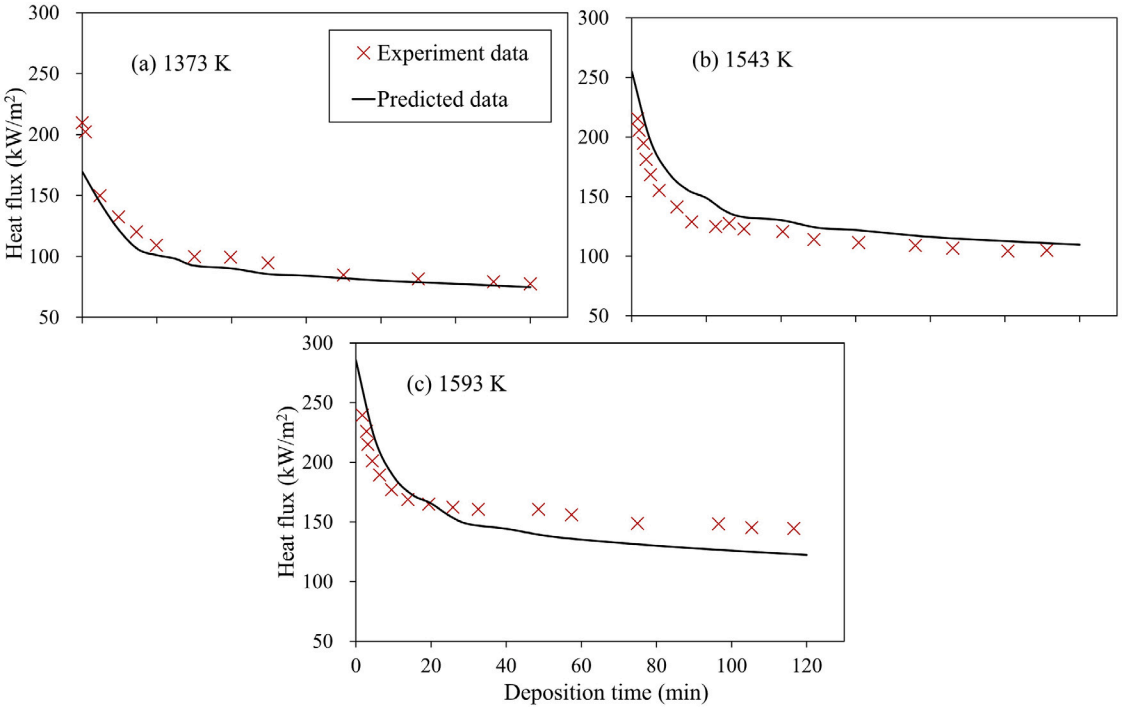

Fig. 6. Comparison of the heat flux between the predicted results and the experimental data as a function of the deposition time under three different furnace temperatures.

because the employment of the mesh smoothing methods would re-distribute the thickness to the adjacent mesh faces. Meanwhile, the smoothing method 2, which contains a group-averaged redistribution algorithm, would spread more thickness to the neighbouring faces during the simulation. Fig. 7(a)–(c) shows that increasing the furnace temperature causes the slight increase in the deposition thickness, and that may be a result of the larger sticking efficiency under the higher furnace temperature. In addition, it can be observed that the increase in the flue gas velocity leads to a significant increase in the deposition thickness, shown in Fig. 7(d)–(f). For instance, the predicted deposition thickness for the cases without smoothing at the deposition time of 2 h increases from 5.8 to 16.3 mm when the flue gas velocity increases from 2.8 to 15 m/s. This is mainly because that the higher flue gas velocity would lead to the higher arrival rate of the ash particles. Furthermore, as shown in Fig. 7(g)–(i), increasing the ash particle size may increase the arrival rate of the ash particles, which would lead to the increase in the deposition thickness as well. At the deposition time of 2 h, the predicted deposition thickness for the cases without smoothing increases from 1.5 to 7.5 mm when the mean particle size increases from 5 to 25 μm. For the predicted results with the smoothing method 1, the mean differences of the deposition thickness are approximately 7.0% to 8.3% compared to the results without the smoothing methods, and the differences of the deposition thickness at 2 h deposition time are around 8.6% to 12.7%. Additionally, the predictions with the smoothing method 2 have larger differences with the mean difference being around 9.2% to 10.7% and the differences of the deposition thickness at 2 h varied from 11.9% to 16.8%. It can be seen that the differences of the predicted deposition thickness between the cases with and without the smoothing methods would become larger over the deposition time. For instance, Fig. 7(b) shows that the difference of the deposition thickness between the cases with smoothing method 1 and without the smoothing is approximately 6.4% at the deposition time of 5 min and then increases to 12.5% at the deposition time of 2 h, respectively.

Fig. 8 shows the predicted heat flux with different mesh smoothing methods under different furnace operational conditions. Generally, the predicted heat flux would decrease rapidly in the initial stage (around 20 min to 30 min) and then slowly decrease in the later stage. The similar variance trends can be observed in both Fig. 8(a)–(i) as well. Fig. 8(a)–(c) shows that a higher furnace temperature results in a higher heat flux. In Fig. 8(d)–(f), increasing the flue gas velocity leads to the increase in the heat flux at the clean tube. The predicted heat flux deceases most significantly under the flue gas velocity of 15 m/s, which would be the result of a fastest increase in the deposition thickness under this condition. As shown in Fig. 8(g)–(i), the predicted heat flux deceases slowly when the mean diameter of the ash particles is 5 μm. This is mainly because the rate of change of the deposition thickness is smaller under the d_{mean} of the ash particles being 5 μm. It is noted that the employment of the mesh smoothing methods has a negligible effect on predicting the heat flux, since the differences between the cases with and without the smoothing methods are less than 3.0% under different furnace operational conditions.

Fig. 9 shows the predicted deposition rate with different mesh smoothing methods under different furnace operation conditions. Fig. 9(a) shows that the predicted deposition rate for the case without the smoothing increases from 355.8 to 451.5 g/(m² h) with increasing the furnace temperature from 1373 to 1593 K. When the flue gas velocity increases from 2.8 to 15 m/s, the predicted deposition rate for the case without the smoothing has a significant increase from 438.2 to 1607.6 g/(m² h), as shown in Fig. 9(b). In addition, it can be observed that the predicted deposition rate for the case without the smoothing increases from 98.5 to 576.7 g/(m² h) when the d_{mean} of the ash particles increases from 5 to 25 μm in Fig. 9(c). The predicted results for the cases with the smoothing methods follow the similar variance trends. Furthermore, the differences of the predicted deposition rate between the cases with and without the mesh smoothing methods are also negligible, which are less than 3.0% under different furnace operational conditions.

4.3. Remarks on mesh smoothing methods

In this paper, the effects of two mesh smoothing methods have been investigated under different furnace operational conditions. The mesh smoothing methods could provide an efficient and stable simulation

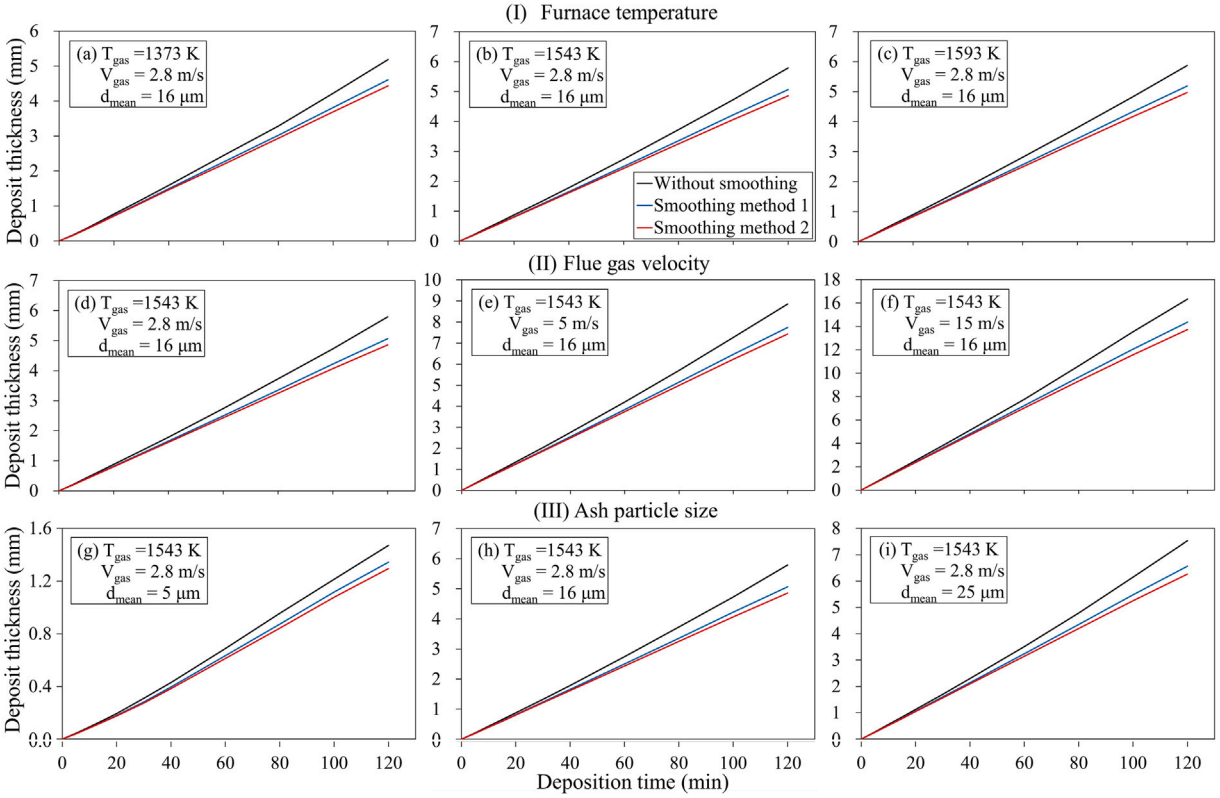

Fig. 7. Comparison of the predicted deposition thickness as a function of the deposition time with different mesh smoothing methods under different furnace operation conditions: (I) Furnace temperature; (II) Flue gas velocity; (III) Ash particle size.

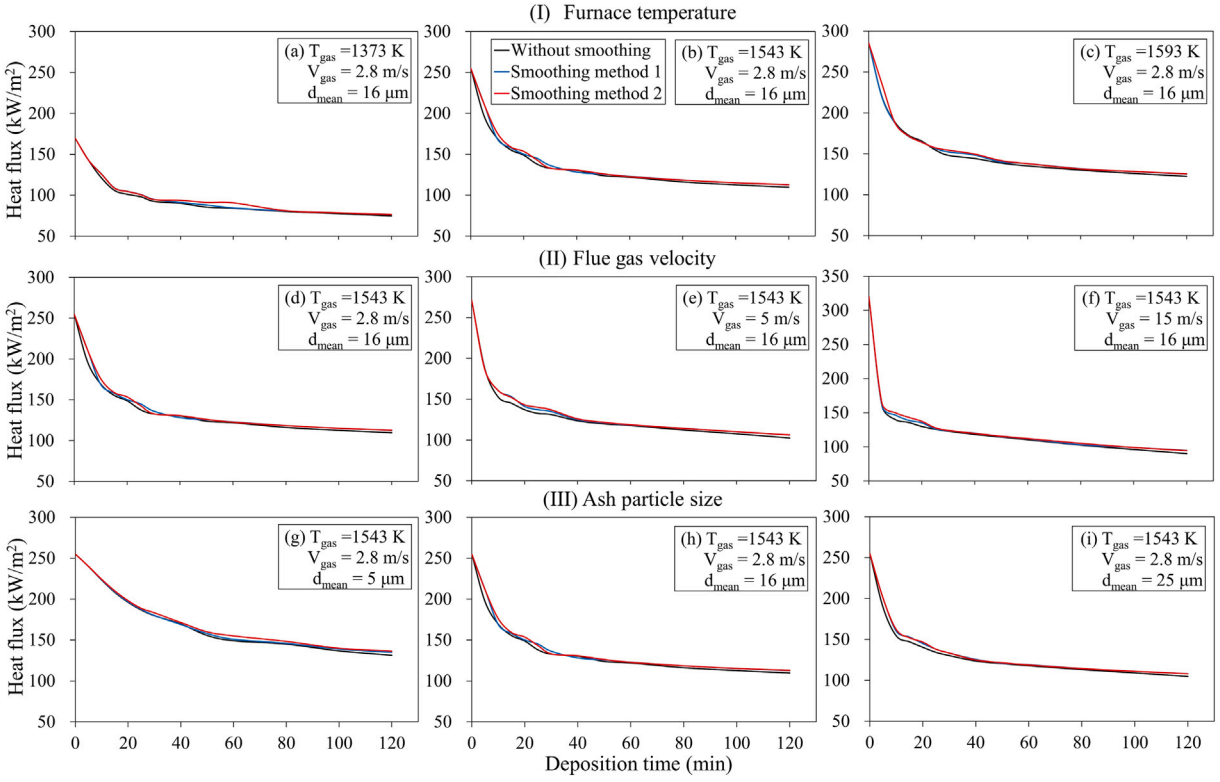

Fig. 8. Comparison of the predicted heat flux as a function of the deposition time with different mesh smoothing methods under different furnace operation conditions: (I) Furnace temperature; (II) Flue gas velocity; (III) Ash particle size.

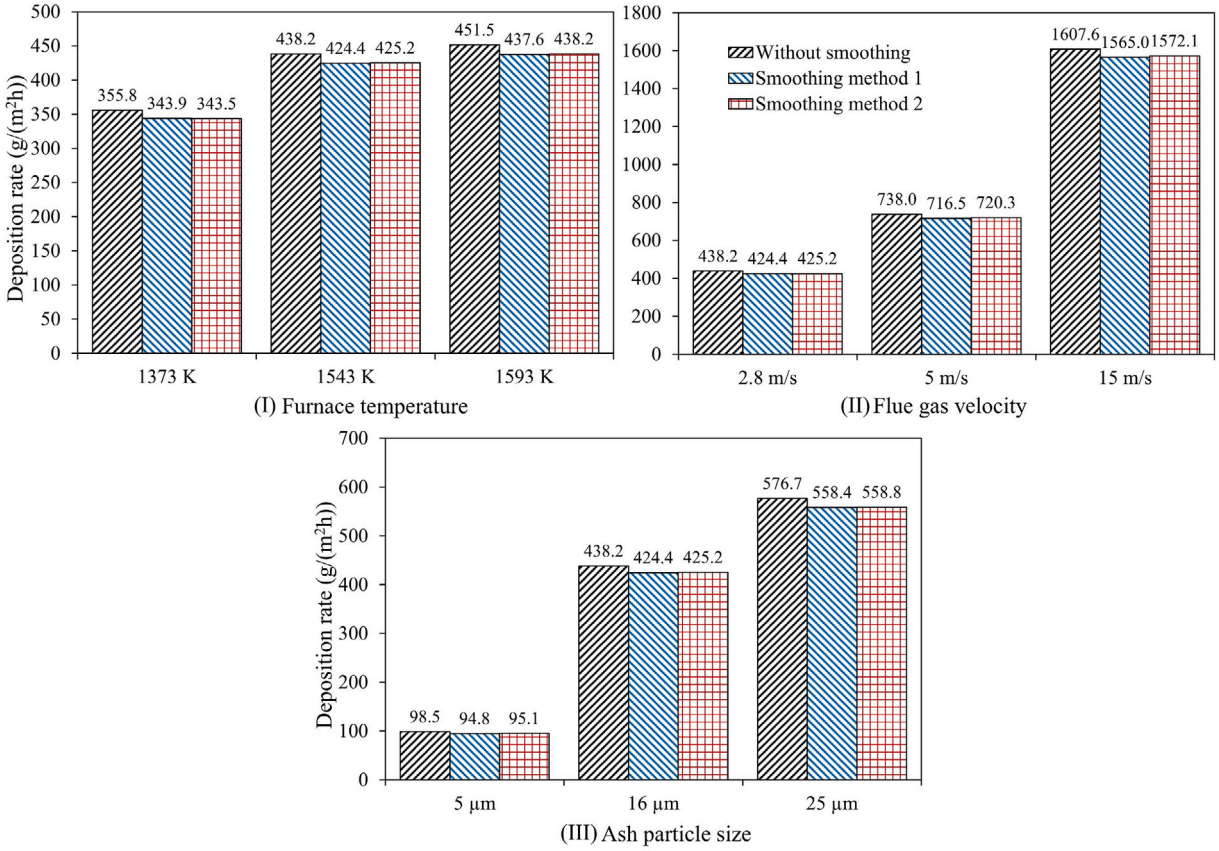

Fig. 9. Comparison of the predicted ash deposition rate with different mesh smoothing methods under different furnace operation conditions: (I) Furnace temperature; (II) Flue gas velocity; (III) Ash particle size.

with a less tracked particle count needed. The employment of the mesh smoothing methods during the simulation has a negligible effect on predicting the heat flux and deposition rate, since the differences between the cases with and without the smoothing methods are less than 3.0% under different furnace operation conditions. Additionally, the applying of the mesh smoothing methods would gently change the predicted deposition shape, especially around the tube position of $\alpha = 180°$. For instance, Fig. 10 shows the predicted ash deposition shape at 2 h deposition time with and without mesh smoothing methods in the baseline case. It can be observed that the predicted deposition shape with the mesh smoothing methods is flatter than the deposition shape without the mesh smoothing methods. More details about the effects of the mesh smoothing methods on the predicted deposition shape under different furnace operation conditions can be found in Appendix D. Employing the mesh smoothing methods in the simulation also makes a clear difference on the predicted deposition thickness at the tube position of $\alpha = 180°$. At the deposition time of 2 h, the differences of the deposition thickness between the cases with and without the smoothing methods could reach to 16.8%. As a result, it needs care when using the mesh smoothing methods when focusing on the deposition thickness.

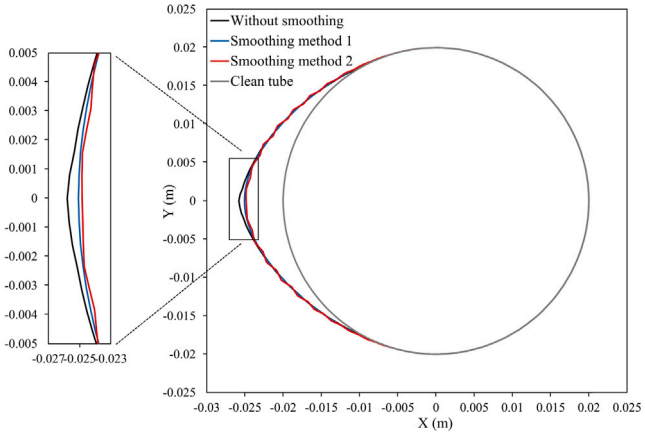

Fig. 10. Comparison of the predicted deposition shape at 2 h deposition time with different mesh smoothing methods in the baseline case ($T_{gas} = T_{par} = 1543$ K, $V_{gas} = 2.8$ m/s, $d_{mean} = 16$ μm).

5. Conclusions

A dynamic CFD model, which combines with the molten fraction based sticking model and the dynamic mesh model, is developed and validated in Zhundong lignite combustion in a pilot-scale furnace. A smooth growth of the deposition and an accurate and stable simulation can be achieved with the employment of this model. The predictions of the heat flux are in reasonable agreement with the experimental data under three different furnace temperatures.

The effects of two mesh smoothing methods have been investigated under different furnace operation conditions. Compared to the simulations without the smoothing methods, a smaller particle count is required during the simulation to obtain the accurate, efficient and stable predicted results. The smoothing methods only produce a small difference (within 3.0%) on the predicted heat flux and deposition rate. In contrast, the deposition thickness at the tube position $\alpha = 180°$ after two deposition hours would be less than 16.8% smaller when compared

to the predicted results without the smoothing methods. Therefore, it requires care in the use of the mesh smoothing methods when focusing on the predictions of the deposition thickness.

CRediT authorship contribution statement

Yufei Tian: Writing – review & editing, Writing – original draft, Validation, Software, Methodology, Investigation, Conceptualization. **Xin Yang:** Writing – review & editing, Methodology, Investigation, Conceptualization. **Lin Ma:** Writing – review & editing, Supervision, Project administration. **Derek Ingham:** Writing – review & editing, Supervision, Project administration. **Mohamed Pourkashanian:** Supervision, Resources, Project administration.

Declaration of competing interest

The authors declare that they have no known competing financial interests or personal relationships that could have appeared to influence the work reported in this paper.

Data availability

The authors are unable or have chosen not to specify which data has been used.

Acknowledgements

Xin Yang would like to acknowledge the National Natural Science Foundation of China (Grants No. 12302327).

Appendix A. Current mesh smoothing methods

The smoothing strategy developed by García Pérez et al. [27], which is applied on the mass distribution, is to ensure the appearance of negative cells is avoided during the simulation. The smoothing scheme can involve a filtering algorithm, which regulates how the mass is distributed around the surface. To be more precise, suppose a particle of mass m is deposited on a face j. The filtering algorithm then redistribute m over the four neighbouring faces, namely the $j-2, j-1, j, j+1, j+2$ faces with a weight ratio $1:2:3:2:1$ [27,40]. Then the redistributed mass $\bar{m}$ on the face j is $\bar{m} = \frac{1}{9}m_{j-2} + \frac{2}{9}m_{j-1} + \frac{3}{9}m_j + \frac{2}{9}m_{j+1} + \frac{1}{9}m_{j+2}$. By implementing this algorithm into the mass distribution, the faces with high collected mass value will share the mass among their neighbouring faces and the faces without any mass can still receive the mass from their neighbours. After applying this filtering algorithm in succession, the resulting mass distribution would appear to be uniform and to approach the average mass collected in the deposit surface [27]. In this study, 10 times application of this filtering algorithm is chosen.

Another smoothing method, developed and applied by Zhou et al. [30,41], is a two-step strategy applied on the thickness of the ash deposition. The first step is to divide the grid faces on the interface into 50 groups and then calculate the averaged increased thickness $\Delta\delta_g$ of each group by:

$$\Delta\delta_g = \frac{\sum_{i=1}^{i=n} \Delta\delta_i}{n} \tag{A.1}$$

where $\Delta\delta_i$ with the script from i to n representing the increased thickness of the continuous faces in each group, respectively; n represents the number of faces in the same group, and g refers to the number of groups. Then the growth of each face group is redistributed with a weighting factor as follows:

$$\Delta\bar{\delta}_g = \frac{2\Delta\delta_{g-2} + 3\Delta\delta_{g-1} + 6\Delta\delta_g + 3\Delta\delta_{g+1} + 2\Delta\delta_{g+2}}{16} \tag{A.2}$$

where the $\Delta\delta_g$ with the script from $g-2$ to $g+2$ representing the averaged thickness for five neighbouring groups. Then the motion of the nodes on the interface would be controlled by the smoothed thickness $\Delta\bar{\delta}_g$ of each group.

Appendix B. Operating conditions of the cases

See Table B.2.

Appendix C. Comparison of the ash deposition properties in the baseline case under different tracked particle counts

Figs. C.11 and C.12 shows the predicted ash deposition properties (deposition shape, deposition thickness, heat flux and deposition rate) with two different mesh smoothing methods under three different particle counts, namely $N, 0.5N$ and $0.25N$. The predicted results of the particle count N without mesh smoothing methods is also shown in these figures. It can be observed that the differences in the deposition shape mainly occur in the leading point of the deposition when the mesh smoothing methods are applied in the simulation (shown in Figs. C.11(a) and C.12(a)). The deposition shapes are smooth with smoothing method 1 under three different particle counts, whilst the shapes are less smooth with smoothing method 2, which is mainly because the smoothing algorithms are different in these two methods. As for the deposition thickness, the lines represented the results of the cases with the smoothing methods are always lower than the black line that refers to the predicted result of the case without the smoothing. Meanwhile, the deposition thickness decreases with the reduction in the particle count both in Figs. C.11(b) and C.12(b). The difference of the deposition thickness at 2 h deposition time between the cases with smoothing method 1 and without the smoothing decreases from 20.1% to 9.8% when the particle count increases from $0.25N$ to N, whilst the difference decreases from 22.5% to 13.7% for the smoothing method 2. As for the predicted heat flux, the mean difference between the cases with and without the smoothing methods are both less than 3.0% under three different particle counts. When employing the smoothing method 1, the predicted deposition rate decreases from 436.2 to 397.6 $g/(m^2\,h)$ with decreasing the particle counts from N to $0.25N$, and the difference increases from 0.5% to 9.3% compared to the predicted results 438.2 $g/(m^2\,h)$ for the case without the smoothing. When it comes to smoothing method 2, the predicted deposition rate decreases from 436.8 to 398.8 $g/(m^2\,h)$ when the particle counts decrease from N to $0.25N$, and the difference increases from 0.3% to 9.0%. When the particle count is $0.5N$, the differences of the predicted deposition thickness, heat flux and deposition rate are both less than 3.0% compared to the results with particle count N with smoothing method 1 and 2. Therefore, the particle count of $0.5N$ is used in the cases with mesh smoothing methods to reduce the simulation cost.

Appendix D. Comparison of the predicted deposition shape at 2 h deposition time with different mesh smoothing methods under different furnace operation conditions

Fig. D.13 shows the predicted deposition shape at 2 h deposition time with different mesh smoothing methods under different furnace operational conditions. Generally, it can be seen that the deposition mainly occurs at the windward section of the tube and the largest thickness of the deposition is at the tube position of $\alpha = 180°$ in both Fig. D.13(a)–(i). The deposition shape characteristics are relatively close to the deposition thickness discussed in Section 4.2. In addition, it can be observed that the differences in the deposition shape with and without the mesh smoothing methods mainly occur around the leading point of the tube. It is mainly because the employment of the mesh smoothing methods would redistribute the thickness to the adjacent mesh faces. Meanwhile, it is noted that the deposition shape with the smoothing method 2 is less smooth, which is mainly because that the smoothing method 2 contains a group-averaged redistribution algorithm.

Table B.2
Operating conditions of the cases.

No.	T_{gas} (K)	T_{par} (K)	V_{gas} (m/s)	Particle Count	d_{mean} (μm)	Smoothing methods
1[a]	1543	1543	2.8	N	16	Without smoothing
2	1543	1543	2.8	$0.5N$	16	Without smoothing
3	1543	1543	2.8	$0.25N$	16	Without smoothing
4	1543	1543	2.8	N	16	Smoothing method 1
5	1543	1543	2.8	$0.5N$	16	Smoothing method 1
6	1543	1543	2.8	$0.25N$	16	Smoothing method 1
7	1543	1543	2.8	N	16	Smoothing method 2
8	1543	1543	2.8	$0.5N$	16	Smoothing method 2
9	1543	1543	2.8	$0.25N$	16	Smoothing method 2
10[a]	1373	1373	2.8	N	16	Without smoothing
11	1373	1373	2.8	$0.5N$	16	Without smoothing
12	1373	1373	2.8	$0.25N$	16	Without smoothing
13	1373	1373	2.8	N	16	Smoothing method 1
14	1373	1373	2.8	$0.5N$	16	Smoothing method 1
15	1373	1373	2.8	$0.25N$	16	Smoothing method 1
16	1373	1373	2.8	N	16	Smoothing method 2
17	1373	1373	2.8	$0.5N$	16	Smoothing method 2
18	1373	1373	2.8	$0.25N$	16	Smoothing method 2
19[a]	1593	1593	2.8	N	16	Without smoothing
20	1593	1593	2.8	$0.5N$	16	Without smoothing
21	1593	1593	2.8	$0.25N$	16	Without smoothing
22	1593	1593	2.8	N	16	Smoothing method 1
23	1593	1593	2.8	$0.5N$	16	Smoothing method 1
24	1593	1593	2.8	$0.25N$	16	Smoothing method 1
25	1593	1593	2.8	N	16	Smoothing method 2
26	1593	1593	2.8	$0.5N$	16	Smoothing method 2
27	1593	1593	2.8	$0.25N$	16	Smoothing method 2
28	1543	1543	5.0	N	16	Without smoothing
29	1543	1543	5.0	$0.5N$	16	Without smoothing
30	1543	1543	5.0	$0.25N$	16	Without smoothing
31	1543	1543	5.0	N	16	Smoothing method 1
32	1543	1543	5.0	$0.5N$	16	Smoothing method 1
33	1543	1543	5.0	$0.25N$	16	Smoothing method 1
34	1543	1543	5.0	N	16	Smoothing method 2
35	1543	1543	5.0	$0.5N$	16	Smoothing method 2
36	1543	1543	5.0	$0.25N$	16	Smoothing method 2
37	1543	1543	15.0	N	16	Without smoothing
38	1543	1543	15.0	$0.5N$	16	Without smoothing
39	1543	1543	15.0	$0.25N$	16	Without smoothing
40	1543	1543	15.0	N	16	Smoothing method 1
41	1543	1543	15.0	$0.5N$	16	Smoothing method 1
42	1543	1543	15.0	$0.25N$	16	Smoothing method 1
43	1543	1543	15.0	N	16	Smoothing method 2
44	1543	1543	15.0	$0.5N$	16	Smoothing method 2
45	1543	1543	15.0	$0.25N$	16	Smoothing method 2
46	1543	1543	2.8	N	5	Without smoothing
47	1543	1543	2.8	$0.5N$	5	Without smoothing
48	1543	1543	2.8	$0.25N$	5	Without smoothing
49	1543	1543	2.8	N	5	Smoothing method 1
50	1543	1543	2.8	$0.5N$	5	Smoothing method 1
51	1543	1543	2.8	$0.25N$	5	Smoothing method 1
52	1543	1543	2.8	N	5	Smoothing method 2
53	1543	1543	2.8	$0.5N$	5	Smoothing method 2
54	1543	1543	2.8	$0.25N$	5	Smoothing method 2
55	1543	1543	2.8	N	25	Without smoothing
56	1543	1543	2.8	$0.5N$	25	Without smoothing
57	1543	1543	2.8	$0.25N$	25	Without smoothing
58	1543	1543	2.8	N	25	Smoothing method 1
59	1543	1543	2.8	$0.5N$	25	Smoothing method 1
60	1543	1543	2.8	$0.25N$	25	Smoothing method 1
61	1543	1543	2.8	N	25	Smoothing method 2
62	1543	1543	2.8	$0.5N$	25	Smoothing method 2
63	1543	1543	2.8	$0.25N$	25	Smoothing method 2

[a] Represents the cases used in the model validation.

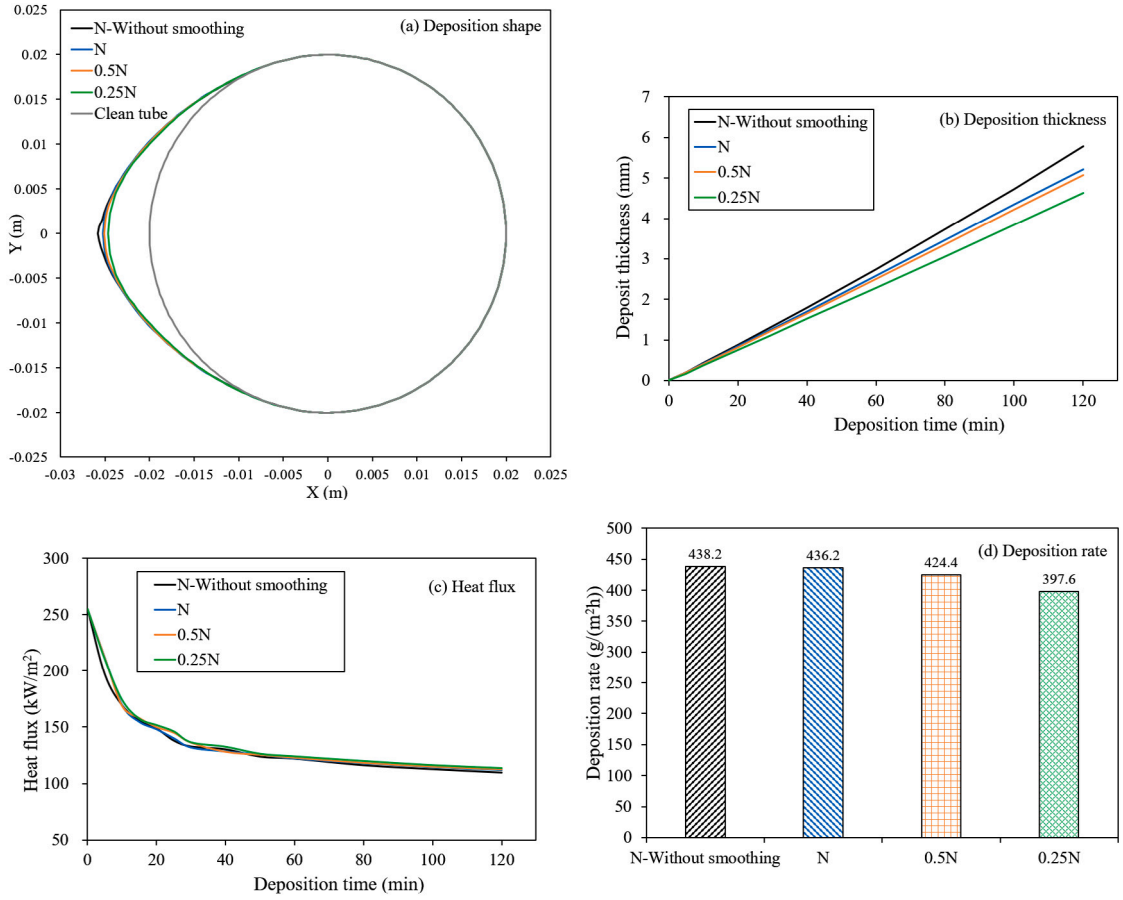

Fig. C.11. Comparison of the predicted ash deposition properties with smoothing method 1 under different particle counts: (a) deposition shape at 2 h deposition time; (b) deposition thickness; (c) heat flux; (d) deposition rate.

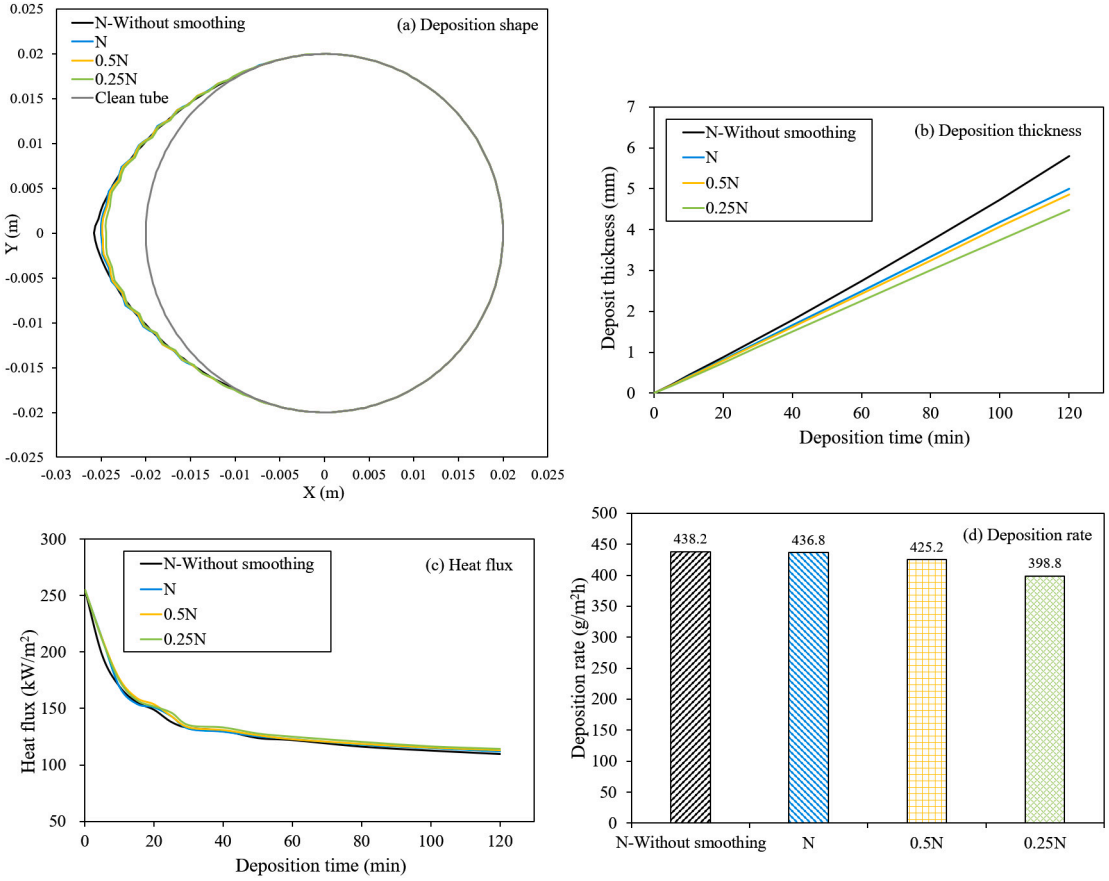

Fig. C.12. Comparison of the predicted ash deposition properties with smoothing method 2 under different particle counts: (a) deposition shape at 2 h deposition time; (b) deposition thickness; (c) heat flux; (d) deposition rate.

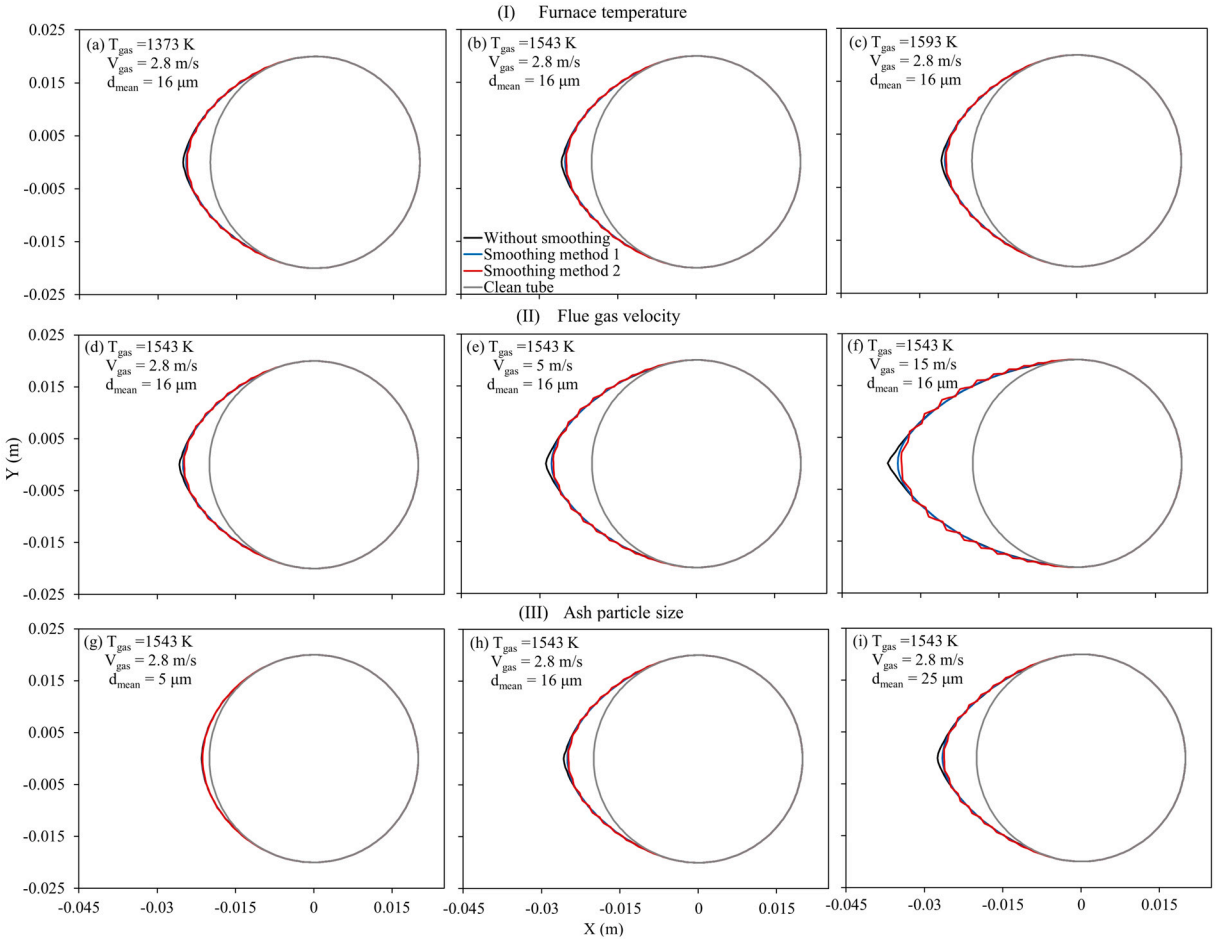

Fig. D.13. Comparison of the predicted deposition shape at 2 h deposition time with different mesh smoothing methods under different furnace operation conditions: (I) Furnace temperature; (II) Flue gas velocity; (III) Ash particle size.

References

[1] BP. BP energy outlook 2022 edition. 2022.

[2] Weber R, Mancini M, Schaffel-Mancini N, Kupka T. On predicting the ash behaviour using computational fluid dynamics. Fuel Process Technol 2013;105:113–28. http://dx.doi.org/10.1016/j.fuproc.2011.09.008.

[3] Yang X. Development of ash deposition prediction models through the CFD methods and the ash deposition indice [Ph.D. thesis], University of Sheffield; 2017, URL https://etheses.whiterose.ac.uk/17127/.

[4] Garba M, Ingham D, Ma L, Degereji M, Pourkashanian M, Williams A. Modelling of deposit formation and sintering for the co-combustion of coal with biomass. Fuel 2013;113:863–72. http://dx.doi.org/10.1016/J.FUEL.2012.12.065.

[5] Bryers RW. Fireside slagging, fouling, and high-temperature corrosion of heat-transfer surface due to impurities in steam-raising fuels. Prog Energy Combust Sci 1996;22:29–120. http://dx.doi.org/10.1016/0360-1285(95)00012-7.

[6] Zbogar A, Frandsen F, Jensen PA, Glarborg P. Shedding of ash deposits. Prog Energy Combust Sci 2009;35:31–56. http://dx.doi.org/10.1016/j.pecs.2008.07.001.

[7] Nunes LJ, Matias JC, Catalão JP. Biomass combustion systems: A review on the physical and chemical properties of the ashes. Renew Sustain Energy Rev 2016;53:235–42. http://dx.doi.org/10.1016/j.rser.2015.08.053.

[8] Roy R, Schooff B, Li X, Montgomery S, Tuttle J, Wendt JO, et al. Ash aerosol particle size distribution, composition, and deposition behavior while co-firing coal and steam-exploded biomass in a 1.5 MW_{th} combustor. Fuel Process Technol 2023;243. http://dx.doi.org/10.1016/j.fuproc.2023.107674.

[9] Tomeczek J, Wacławiak K. Two-dimensional modelling of deposits formation on platen superheaters in pulverized coal boilers. Fuel 2009;88:1466–71. http://dx.doi.org/10.1016/j.fuel.2009.02.023.

[10] Fei Y. Computational fluid dynamics and process co-simulation applied to carbon capture technologies [Ph.D. thesis], University of Leeds; 2015, URL https://etheses.whiterose.ac.uk/11521/.

[11] ANSYS FLUENT 19.2 theory guide. ANSYS Inc.; 2018.

[12] Yang X, Ingham D, Ma L, Zhou H, Pourkashanian M. Understanding the ash deposition formation in Zhundong lignite combustion through dynamic CFD modelling analysis. Fuel 2017;194:533–43. http://dx.doi.org/10.1016/j.fuel.2017.01.026.

[13] Weber R, Schaffel-Mancini N, Mancini M, Kupka T. Fly ash deposition modelling: Requirements for accurate predictions of particle impaction on tubes using RANS-based computational fluid dynamics. Fuel 2013;108:586–96. http://dx.doi.org/10.1016/J.FUEL.2012.11.006.

[14] Wieland C, Kreutzkam B, Balan G, Spliethoff H. Evaluation, comparison and validation of deposition criteria for numerical simulation of slagging. Appl Energy 2012;93:184–92. http://dx.doi.org/10.1016/J.APENERGY.2011.12.081.

[15] Walsh PM, Sayre AN, Loehden DO, Monroe LS, Beér JM, Sarofim AF. Deposition of bituminous coal ash on an isolated heat exchanger tube: Effects of coal properties on deposit growth. Prog Energy Combust Sci 1990;16:327–45. http://dx.doi.org/10.1016/0360-1285(90)90042-2.

[16] Srinivasachar S, Senior CL, Helble JJ, Moore JW. A fundamental approach to the prediction of coal ash deposit formation in combustion systems. Symp (Int) Combust 1992;24:1179–87. http://dx.doi.org/10.1016/S0082-0784(06)80139-6.

[17] Huang LY, Norman JS, Pourkashanian M, Williams A. Prediction of ash deposition on superheater tubes from pulverized coal combustion. Fuel 1996;75:271–9. http://dx.doi.org/10.1016/0016-2361(95)00220-0.

[18] Wang H, Harb JN. Modeling of ash deposition in large-scale combustion facilities burning pulverized coal. Prog Energy Combust Sci 1997;23:267–82. http://dx.doi.org/10.1016/s0360-1285(97)00010-5.

[19] Rushdi A, Gupta R, Sharma A, Holcombe D. Mechanistic prediction of ash deposition in a pilot-scale test facility. Fuel 2005;84:1246–58. http://dx.doi.org/10.1016/J.FUEL.2004.08.027.

[20] Degereji MU, Ingham DB, Ma L, Pourkashanian M, Williams A. Prediction of ash slagging propensity in a pulverized coal combustion furnace. Fuel 2012;101:171–8. http://dx.doi.org/10.1016/j.fuel.2010.12.038.

[21] Taha TJ, Stam AF, Stam K, Brem G. CFD modeling of ash deposition for co-combustion of MBM with coal in a tangentially fired utility boiler. Fuel Process Technol 2013;114:126–34. http://dx.doi.org/10.1016/J.FUPROC.2013.03.042.

[22] Ai W, Kuhlman JM. Simulation of coal ash particle deposition experiments. Energy Fuels 2011;25:708–18. http://dx.doi.org/10.1021/EF101294F.

[23] Brach RM, Dunn PF. A mathematical model of the impact and adhesion of microsphers. Aerosol Sci Technol 1992;16:51–64. http://dx.doi.org/10.1080/02786829208959537.

[24] Li G, Li S, Huang Q, Yao Q. Fine particulate formation and ash deposition during pulverized coal combustion of high-sodium lignite in a down-fired furnace. Fuel 2015;143:430–7. http://dx.doi.org/10.1016/j.fuel.2014.11.067.
[25] Cai Y, Tay K, Zheng Z, Yang W, Wang H, Zeng G, et al. Modeling of ash formation and deposition processes in coal and biomass fired boilers: A comprehensive review. Appl Energy 2018;230:1447–544. http://dx.doi.org/10.1016/J.APENERGY.2018.08.084.
[26] Kær SK, Rosendahl LA, Baxter LL. Towards a CFD-based mechanistic deposit formation model for straw-fired boilers. Fuel 2006;85:833–48. http://dx.doi.org/10.1016/J.FUEL.2005.08.016.
[27] García Pérez M, Vakkilainen E, Hyppänen T. 2D dynamic mesh model for deposit shape prediction in boiler banks of recovery boilers with different tube spacing arrangements. Fuel 2015;158:139–51. http://dx.doi.org/10.1016/j.fuel.2015.04.074.
[28] García Pérez M, Vakkilainen E, Hyppänen T. Fouling growth modeling of kraft recovery boiler fume ash deposits with dynamic meshes and a mechanistic sticking approach. Fuel 2016;185:872–85. http://dx.doi.org/10.1016/j.fuel.2016.08.045.
[29] Yang X, Zhou H, Wu H. CFD modelling of biomass ash deposition under multiple operation conditions using a 2D mass-conserving dynamic mesh approach. Fuel 2022;316:123250. http://dx.doi.org/10.1016/J.FUEL.2022.123250.
[30] Zhou H, Zhang K, Li Y, Zhang J, Zhou M. Simulation of ash deposition in different furnace temperature with a 2D dynamic mesh model. J Energy Inst 2019;92:1743–56. http://dx.doi.org/10.1016/J.JOEI.2018.12.006.
[31] Zheng Z, Yang W, Yu P, Cai Y, Zhou H, Boon SK, et al. Simulating growth of ash deposit in boiler heat exchanger tube based on CFD dynamic mesh technique. Fuel 2020;259:116083. http://dx.doi.org/10.1016/J.FUEL.2019.116083.
[32] Mueller C, Selenius M, Theis M, Skrifvars BJ, Backman R, Hupa M, et al. Deposition behaviour of molten alkali-rich fly ashes—development of a submodel for CFD applications. Proc Combust Inst 2005;30:2991–8. http://dx.doi.org/10.1016/J.PROCI.2004.08.116.
[33] Richards GH, Slater PN, Harb JN. Simulation of ash deposit growth in a pulverized coal-fired pilot scale reactor. Energy Fuels 1993;7:774–81. http://dx.doi.org/10.1021/EF00042A012.
[34] Li QH, Zhang YG, Meng AH, Li L, Li GX. Study on ash fusion temperature using original and simulated biomass ashes. Fuel Process Technol 2013;107:107–12. http://dx.doi.org/10.1016/j.fuproc.2012.08.012.
[35] Li B, Brink A, Hupa M. CFD investigation of deposition in a heat recovery boiler: Part II - Deposit growth modelling. Prog Comput Fluid Dyn 2009;9:453–9. http://dx.doi.org/10.1504/PCFD.2009.027763.
[36] Zheng Z, Yang W, Cai Y, Wang Q, Zeng G. Dynamic simulation on ash deposition and heat transfer behavior on a staggered tube bundle under high-temperature conditions. Energy 2020;190:116390. http://dx.doi.org/10.1016/J.ENERGY.2019.116390.
[37] Zhou H, Zhou B, Li L, Zhang H. Experimental measurement of the effective thermal conductivity of ash deposit for high sodium coal (Zhundong coal) in a 300 kW test furnace. Energy Fuels 2013;27:7008–22. http://dx.doi.org/10.1021/ef4012017.
[38] Greifzu F, Kratzsch C, Forgber T, Lindner F, Schwarze R. Assessment of particle-tracking models for dispersed particle-laden flows implemented in OpenFOAM and ANSYS FLUENT. Eng Appl Comput Fluid Mech 2016;10:30–43. http://dx.doi.org/10.1080/19942060.2015.1104266.
[39] Yang X, Szuhánszki J, Tian Y, Ingham D, Ma L, Pourkashanian M. Understanding the effects of oxyfuel combustion and furnace scale on biomass ash deposition. Fuel 2019;247:36–46. http://dx.doi.org/10.1016/J.FUEL.2019.03.031.
[40] García Pérez M. Modeling the effects of unsteady flow patterns on the fireside ash fouling in tube arrays of kraft and coal-fired boilers [Ph.D. thesis], Lappeenranta University of Technology; 2016, URL https://urn.fi/URN:ISBN:978-952-335-001-4.
[41] Zhou H, Hu S. Numerical simulation of ash deposition behavior with a novel erosion model using dynamic mesh. Fuel 2021;286:119482. http://dx.doi.org/10.1016/J.FUEL.2020.119482.